AD-A142 193 CONCEPTUAL EXPERIMENTS IN TRANSITION TO TURBULENCE THROUGH COMBINED VISUA..(U) ILLINOIS INST OF TECH CHICAGO M V MORKOVIN ET AL. 31 APR 84 ARO-17690.1-EG

UNCLASSIFIED DAAG29-81-K-0012 F/G 20/4 NL

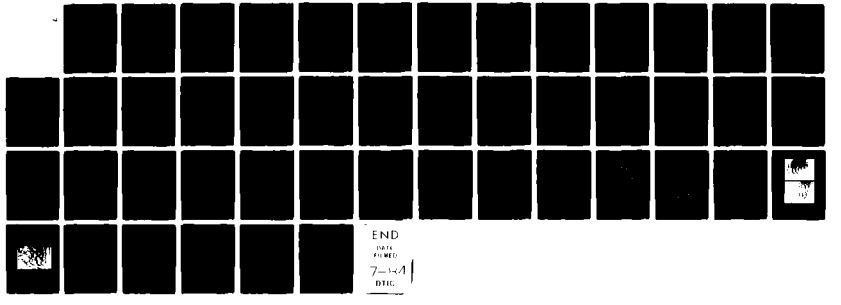

END

DATE FILMED

7-84

DTIC

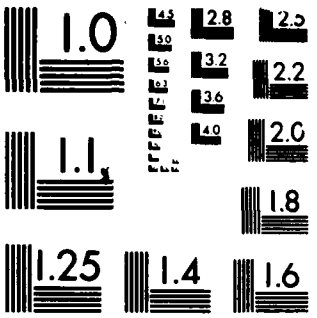

CONCEPTUAL EXPERIMENTS IN TRANSITION TO TURBULENCE THROUGH COMBINED VISUALIZATION AND HOT-WIRE TECHNIQUES

FINAL REPORT

by

M. V. Morkovin and T. C. Corke

April 31, 1984

U.S. ARMY RESEARCH OFFICE

Contract SFRC No. DAAG 29-81-K-0012

Illinois Institute of Technology
Chicago, IL. 60616

Unclassified

SECURITY CLASSIFICATION OF THIS PAGE (When Data Entered)

REPORT DOCUMENTATION PAGE	READ INSTRUCTIONS BEFORE COMPLETING FORM
1. REPORT NUMBER: ARO 17690.1-EG	2. GOVT ACCESSION NO.: AD-A142 193	3. RECIPIENT'S CATALOG NUMBER
4. TITLE (and Subtitle): Conceptual Experiments in Transition to Turbulence through Combined Visualization and Hot-Wire Techniques	5. TYPE OF REPORT & PERIOD COVERED: FINAL REPORT Nov. 1980 - Jan. 1984
	6. PERFORMING ORG. REPORT NUMBER
7. AUTHOR(s): M.V. Morkovin and T. Corke	8. CONTRACT OR GRANT NUMBER(s): SFRC No DAAG 29-81-K-0012
9. PERFORMING ORGANIZATION NAME AND ADDRESS	10. PROGRAM ELEMENT, PROJECT, TASK AREA & WORK UNIT NUMBERS
11. CONTROLLING OFFICE NAME AND ADDRESS: U. S. Army Research Office, Post Office Box 12211, Research Triangle Park, NC 27709	12. REPORT DATE: March 31, 1984
	13. NUMBER OF PAGES
14. MONITORING AGENCY NAME & ADDRESS (if different from Controlling Office)	15. SECURITY CLASS. (of this report): Unclassified
	15a. DECLASSIFICATION/DOWNGRADING SCHEDULE

16. DISTRIBUTION STATEMENT (of this Report)

Approved for public release; distribution unlimited.

17. DISTRIBUTION STATEMENT (of the abstract entered in Block 20, if different from Report)

A-1

DTIC COPY INSPECTED 3

18. SUPPLEMENTARY NOTES

The view, opinions, and/or findings contained in this report are those of the author(s) and should not be construed as an official Department of the Army position, policy, or decision, unless so designated by other documentation

19. KEY WORDS (Continue on reverse side if necessary and identify by block number)

Distributed Roughness
Tollmien-Schlichting Waves
Stability
Laminar Boundary Layers
Transition
Acoustic Forcing

20. ABSTRACT (Continue on reverse side if necessary and identify by block number)

1. Effects of distributed roughness on transition to turbulence. Distributed roughness with nominal height k in a boundary layer with displacement thickness δ^* is known to lead to early non-Tollmien-Schlichting (TS) transition when k/δ^* exceeds unity in non accelerated flows. The question arose whether more commonly occurring milder roughness might not enhance the TS mechanism and also lead to early transition. Extensive hot-wire exploration and

DD FORM 1 JAN 73 1473 EDITION OF 1 NOV 65 IS OBSOLETE

UNCLASSIFIED

SECURITY CLASSIFICATION OF THIS PAGE (When Data Entered)

smoke-wire visualization of flow over smooth and rough walls revealed for the first time that distributed roughness can indeed bring about earlier transition through enhanced TS amplification mechanism. The effect may be three-fold. First, the system of streamwise vortices downstream of the higher roughness elements and the low inertia fluid in the valleys between the elements evidently respond more readily to free-stream disturbances than does the orderly near-wall flow over smooth surfaces. Second, once the TS fluctuations commence, they grow faster. Whether this is due to continued input from free-stream disturbances along the path or to an increased destabilization of the system remains unclear. Third, there is some evidence of roughness induced three-dimensionalization of the wave fronts which leads to secondary subharmonic instability and, hence,to turbulence. These findings throw new and different light on the flows over distributed roughness.

2. Generation of instability waves by external unsteady pressure gradients.
Such generation is an experimental fact but its mechanism and the controlling parameters for the response remained unknown until the present experiments. TS waves grow past Re_{cr} at the circular frequency ω of the excitor but at their own relatively short wavelength λ. When the pressure gradient has a constant amplitude A, the transfer of energy and vorticity from the driving field to the TS field averages out to zero over each TS wavelength. When the amplitude varies with x, A(x), then a non-zero averaged input to the TS field exists, proportional to the spectral intensity of the Fourier transform of A at the TS wavenumber, $A_F(k_{TS})$. Since all practical bodies have finite thickness, the the unsteady pressure gradients diffract around the bodies and thereby incur the requisite A(x) variation. The scenario was verified in a numerical experiment, where in cooperation with H. Fasel, Navier-Stokes equations for a special nonhomogeneous problem were solved by difference techniques. Earlier the concepts were verified in a wind tunnel where a sound source was placed above a boundary layer. A hot-wire documented both the A(x) variation above the BL and the growing TS response within the BL. This project was supported in part by NSF.

3. Generation of TS waves by sound through a hole under the boundary layer.
This prelude to the experiment under (2) intended (a) to clarify the mechanism of generation and (b) to provide needed data for testing three-dimensional TS theory and computational techniques. The diagnostics covering (a) were successfuly completed when a Russian paper by Gilev, Kachanov, and Kozlov covering (b) arrived. Therefore the more routine data collecting (b) was discontinued. As to (a), the amplitude of the unsteady pressure gradients here depends on both x and z, A(x,z) and generates therefore strong interference patterns of three-dimensional TS waves. Furthermore, there is a sharper localized driving source over the small area of the hole itself.

FORWORD

Transition to turbulence intrudes into many practical flow problems. Even when a boundary layer is turbulent on the full scale of a prototype, a misestimate of transition onset often results in errors in skin friction of 20 % or more. Transition also has to be taken into account in projecting full-scale performance from any smaller-scale testing which is always influenced by a different set of environmental disturbances. How environmental disturbances, free-stream turbulence, sound, surface roughness, vibrations etc. lead to instabilities and turbulence is not understood more than 100 years after the discovery of turbulence. Until the many mechanisms in this general problem of boundary-layer receptivity are identified, we shall lack the knowledge of the controling parameters. Relying on correlation of existing sparse reliable transition data when detail controling parameters remain unknown is risky engineering. Under the present contract our understanding of environmental influences has been significantly advanced in the area of distributed roughness and receptivity to unsteady pressure gradients (including sound). Additional publishable results were obtained on the problem of interferance and growth of three-dimensional instability waves caused by a periodic pressure disturbance emanating from a small hole under the boundary layer. Their significance lies in their role as test cases for three-dimensional instability theory. Finally, a number of lessons learned in battling unexpected high environmental disturbances will be reported in a chapter on Environments in Flow Facilities of Morkovin's 1985 book on transition.

The faculty members cooperating on the project were: Mark V. MORKOVIN (presently Emeritus Professor) Principal Investigator throughout the duration of the project, November 1980 through January 1984; Michio NISHIOKA, Visiting Associate Professor, on leave from the University of Osaka Prefecture University, Japan, November 1980 through March 1982. Thomas CORKE (Assistant Professor) Co-principal Investigator, September 1982 through January 1984. Hassan NAGIB (Professor) was a consultant on the roughness project and on combatting environmental disturbances.

The shortage of experimentally oriented graduate students plaguing the country regrettably limited the students working on the project to only two: Michael W. PLESNIAK, (Senior and Graduate student), December 1980 through June 1982; part of his work served as his Senior Research Project. Amir BAR-SEVER, (Graduate student) September 1982 through January 1984; his report will serve as his Master's thesis, May 1984.

A paper on the distributed roughness problem by Corke, Bar-Sever and Morkovin, is planned for submission to the Physics of Fluids.

A note on the evolution three-dimensional disturbance down-stream from a periodically pulsing hole under the boundary layer, by Nishioka and Morkovin, is planned for submission to the Physics of Fluids.

A manuscript by Nishioka and Morkovin on the receptivity of boundary layers to unsteady pressure gradients is undergoing its second revision. It is aimed at the Journal of Fluid Mechanics.

Besides the aformentioned bits and pieces on the environmental disturbances in Morkovin's book, two other related sections entilted "Three-dimensional roughness" and "Distributed roughness effects" will also be included in the book. This critical survey and prognosis is readied to be issued as an Interim Technical Report. The book: "Guide to Experiments on Instability and Laminar-Turbulent Transition in Shear Layers", is slated for publication by AIAA in June 1985. About one fourth of the material is available from National Technical Information Service as AFOSR-TR-83-0931, AD-A134796 under the title "Understanding Transition to Turbulence in Shear Layers".

A short presentation on the sound reseptivity titled: "Excitation of TS waves by unsteady preasure gradients" was made by Morkovin at a meeting of the American Physical Society in Houston in November 1983. The associated abstract by Nishioka and Morkovin appeared on page 1372 of the Bulletin of the American Physical Society, Vol. 28, No. 9, Nov. 1983.

In this Final Report the work on the roughness is discussed first and in considerable detail. In view of the imminent availability of the JFM manuscript on the sound receptivity, a more concise description of that work is offered here.

TABLE OF CONTENTS

LIST OF TABLES AND FIGURES

I. EFFECTS OF DISTRIBUTED ROUGHNESS ON TRANSITION

1.1 Isolated 2D and 3D roughness fields

Effects of roughness of height k must depend on its relative height, k/δ^*, (δ^* = boundary-layer displacement thickness) or its nominal dimensionless disturbance to the flow near the wall, Re_k, or both; ($Re_k = kU_k/\nu$, where U_k is the undisturbed velocity at height k and ν the kinematic viscosity; for Blasius boundary layers and small k values $Re_k = 0.57Re_{\delta^*}(k/\delta^*)^2$). Two-dimensional isolated roughness, such as a spanwise trip wire, causes local upstream and downstream separations, the latter extending 40k-50k before reattachment to the wall. The separated inflectional velocity profiles amplify Tollmien-Schlichting (TS) instability waves very much more rapidly than the undisturbed boundary layer, Ref. 1. This powerful overamplification makes trip wires most efficient in causing early transition -- through a well understood and hence partially controllable mechanism.

The relevance of an isolated 2D roughness to the problem of distributed roughness lies in the fact that in most experiments on distributed roughness, strips or sheets of abrasive paper fastened to the wall provide the roughened surface. In so far as the substrate and granules form quasi-two-dimensional protuberances at the leading and trailing edges, some of the powerful 2D-isolated-roughness mechanism is operative. These leading and trailing-edge effects of roughness patches have complicated the correlations of data from past experiments. Thus $(k/\delta^*)_0$ and Re_{k0} values at the leading edge, x/k_0, have special risk significance beyond the connotations of k/δ^* and Re_{δ^*} values for an isolated 3D roughness element or for an element in the middle of a roughness patch.

The nature of locally separated regions at a 3D isolated roughness (with nearly equal height, span, and length) differs greatly from that for 2D isolated roughness. The rear pocket is very short: on the order of 5k. The front separation generates a horseshoe vortex which wraps around the roughness, forming streamwise vortices which induce downwash along the centerlines of the wake. For Re_k below about 300, the separated rear shear layer and the head and legs of the

horseshoe vortex are stable. At higher Re_k values even the short separated rear shear layer becomes unstable and starts shedding downstream moving vortex loops looking like hairpins with the head pointing downstream. The vortex rotation is opposite to that of the horseshoe vortices which are underneath and somewhat to the side of the stretching hairpin arms. The rotation of the hairpin head generates an upward force which progressively moves the head of the loop to the edge of the boundary layer as it floats downstream.

The frequency of the shedding is rather high so that no TS instability is induced in the neighboring boundary layer even past its critical Reynolds number Re_{CrTS}. As Re_k increases, the horseshoe vortices and the stretching interlacing hairpin vortices grow stronger. At Re_k values nearing 550-600 (depending on the x_k), the interaction of this multiple vortex system with the boundary layer causes a sudden local onset of turbulence at first rather far downstream: x_{tr} occurs at $2x_k$ to $5x_k$ or even farther! In other words the incubation distance from the offending roughness to the roughness-conditioned transition is initially very long; furthermore this induction of turbulence bypasses the quasi-two-dimensional TS mechanism. As Re_k grows still higher, x_k moves very rapidly upstream; for an increment of 10 in Re_k, the forward movement of x_{tr} may cover more than half the distance to x_k.

To sum up: transition induced by a single 3D roughness element occurs first at large incubation distances downstream, as an interaction involving a streamwise vortex system, and is then very sensitive to even small increases in Re_k, moving rapidly to the near-wake of the element. The process is therefore vastly different from induction of transition by a single 2D roughness. The significant features of relevance to distributed 3D roughness are (a) the existence of complex, predominantly streamwise vorticity patterns and (b) the existence of long induction distances from the process-initiating roughness to the onset of turbulence. Effect (b) makes the judgement of cause and effect very difficult and dims the prospects for successful schemes of parameter correlation. Bibliography and documentation of the roughness overview in Section 1.1 and part of Section 1.2 is presented in Morkovin's forthcoming Interim Technical

Report and in Sections 0.04.09 and 0.04.10 of his 1985 book.

1.2 Preliminary considerations and recent history of the problem.

What happens to feature (a), the streamwise vorticity systems, when the roughness element has neighbors as in distributed roughness? At present no instrument can measure the interactions between these building blocks of the near-wall flow and their concatenation. Since the elements are more or less randomly distributed, there will certainly be some infringement of the streamwise vorticies from an upstream element upon the horseshoe vortex head wrapped around a downstream element, a potentially destabilizing occurrence. However, if the elements are packed rather closely there will be little upstream fetch to generate a strong horseshoe vortex; with increasing grain density, there is likely to be partially dead fluid in the free space between elements. In any case, much of the fluid in the crooked valleys is likely to have very low velocity (inertia) so that it may be influenced rather easily by free-stream velocity and pressure disturbances. Nearer to the peaks of the elements the fluid will have considerable streamwise vorticity with spanwise scales on the order of k, i.e. rather small relative to δ. Commonly present spanwise nonuniformities in the roughness element distribution may create larger spanwise scales, which could promote amalgamation of the smaller streamwise vortex structures. Such amalgamation is occasionally seen in smooth boundary layers with streamwise vorticity.

The impact of the preceding speculations is that we should expect: (A) some dynamics involving streamwise vorticity, set by the spanwise distribution of the roughness and (B) susceptibility of the lower-inertia fluid in the valleys to free-stream disturbances. Specifically we should allow for the possibility that the same external free-stream disturbances may induce a larger response on our rough surfaces than on our smooth surface.

One scenario was dismissed quite early in our investigations: for the standard sandpaper roughness transition is most unlikely to be triggered by the few highest peaks in the statistical k distribution in the manner described in the preceding Section for the isolated 3D roughness elements. We were observing transition, with smoke wire as

well as hot wire, at Re_k values much too low for the essential shedding of hairpin vortices to take place. Nor were there any evident preferential spanwise locations of laminar-flow breakdown after incubation that would point to fixed highest roughness peaks upstream as the causative agents.

Nevertheless the experience of Leventhal and Reshotho (LR), Ref. 2, indicated that higher k values at smaller x_k locations generated early turbulence. We used the same commercial sandpaper, a fine-grit NORTON Co. paper #80 with nominal k of 0.26 mm and a coarser grit SANCAP Co. paper #24 with nominal k of 1.04 mm. When the sheet of the paper extends to the leading edge of a flat plate, roughness of these magnitudes causes turbulence very early. To study the transition region with adequate spatial resolution it is therefore necessary to introduce a leading edge of the roughness sheet farther downstream as mentioned in Section 1.1. Initially LR placed the leading edge of the 0.26 mm roughness at x_t = 3 cm (Re_{k0} = 33, $(k/\delta^*)_0$ = 0.56, $Re^*_{\delta 0}$ = 190 as quoted at their free-stream velocity U_0 of 6 m/s) and found developed turbulence at their measuring station at x = 30 cm (Re_{δ}^* = 596). Their initial position x_k for the rougher surface was 6.5 cm (Re_{k0} = 314, $(k/_{\delta}{}^*)_0$ = 1.48, Re_{k0} = 285) yielding developed turbulence at the measuring station at x = 20 cm (Re_{δ}^* = 486). Since TS critical $Re^*_{\delta Cr}$ for first amplification over smooth walls is approximately 500 and disturbance amplitudes in the LR wind tunnel had to rise by factors of over a thousand for turbulence to occur, the process leading to turbulence in both cases had to be a non-TS process. This merely confirmed the widely held belief that distributed roughness frequently induces turbulence through an unknown mechanism without involving Tollmien's amplification mechanism. This is consistent with our expectations (A) and (B). A separate important question is whether roughness may influence TS developments when $Re^*_{\delta 0}$ at x_{k0} is closer to $Re^*_{\delta Cr}$ of the TS mechanism.

LR moved the leading edge of their roughness sheets to x_{k0} = 6.5 cm (Re_{k0} = 23, $(k/_{\delta}{}^*)_0$ = 0.38, Re_{δ}^* = 285) and to x_{k0} = 18.3 cm (Re_{k0} = 314, $(k/_{\delta}{}^*)_0$ = 0.88, $Re^*_{\delta 0}$ = 480) for the fine and coarse roughness, respectively. Their hot-wire explorations indicated again no evidence for the involvement of the TS mechanism in the build up of

turbulence. Their search for the possibility of TS involvement was prompted by a phenomenological theory of Merkle, Tzou, and Kubota (Ref. 3) which assumed that the roughness changed the mean-velocity profile into an inflectional one, just above the roughness peaks, a profile that would amplify disturbances much faster than the Blasius layer. The assumption of the inflectional profile is of course correct for the 2D isolated roughness case (Section 1.1) but LR found no evidence of inflection nor of enhanced TS-like amplification. Neither did Shin, Prahl, and Reshotko (Ref. 4) in a water tunnel, where they introduced an upstream vibrating ribbon to make possible measurements of more reliable amplification rates.

An inflection point of the mean profile was observed for the first time by Kendall (Ref. 5). He used a special sampling technique in the most accurate measurements to date for a location where the local Re_k was 31 and the local Blasius coordinate at the top of the roughness was low i.e. 0.36 ($k/\delta^* = 0.21$). From Kendall's profiles we infer that the inflection must have been induced by vertical transfer of u momentum by the streamwise vorticity (expectation A), i.e. by a special eddy viscosity. Our critique of Merkle et al is that in the crucial near-wall region their theory should also use the same effective viscosity and more realistic boundary conditions than those of an undisplaced smooth wall. Kendall also documented destabilizing changes of profiles at the leading and trailing edges of roughness patches as discussed in Section 1.1. However he explored only mean flow effects over and downstream of isolated and distributed roughnesses with small k/δ^* values. Thus there is no indication that his inflected profiles would amplify disturbances faster than the Blasius profile.

1.3 Some research questions and methodology.

The experiments were conducted on the back wall of the IIT Visualization Facility. We were hoping that smoke-wire visualization would provide global information on the possibility of spanwise-preferred upstream breakdown locations and configurations and on the existence of the elusive TS wave fronts. It was used extensively for early diagnostics. It should be remarked that the wake of the thin

smoke wire in a boundary layer modifies the profile for about 8δ-10δ Thus the smoke registers somewhat increased disturbances compared to those in the absence of the wire; see Thomas (Ref. 6).

To shed new light on the delicate question of the degree of contamination of the distributed-roughness effect by the quasi-two-dimensional leading edge of the abrasive paper, we adopted a suggestion of H. Nagib. Since we could not observe clear manifestations of instability with the 0.26 mm roughness, we ran two configurations of the 1.04 mm roughness: protruding and recessed. In the recessed R1 configuration the upstream smooth flat wall was lined up with the peaks of the highest roughnesses; in the protruding R1 configuration the wall was lined up with the substrate of the same roughness sheet. The reference measurements were made on the smooth S configuration of the alined smooth wall.

All configurations were run at two tunnel speeds U_0 = 4.8m/s, designated by L for low, and U_0 = 6.2 m/s, designated by H for high. As can be seen from the comparative Table I the roughness commenced always past the critical Reynolds number of about 500, a distinct difference from the LR experiments. This choice was prompted by our requirement that there be a Blasius profile at the start so that more meaningful comparisons could ensue.

1.4 On mean profiles over rough walls.

The profiles are expected to depart from that of Blasius near the leading edge of the roughness and are unlikely to settle into a similarity family since k/δ^* varies with x. Because of the obstruction from the roughness elements, the hot-wire cannot measure mean velocities much below $0.35U_0$ so that a good portion of the profiles requires extrapolation. The technique for inferring an effective wall location with U=0 is outlined in the Appendix. The method follows that of L&R; we confirm their finding that the hot wire invariably gives reasonable and consistent readings for part of the range $k_{nom} < k_{max}$. The smooth extrapolation to U=0 rests on three to five innermost points which are deemed to be in the region where U is linearly proportional to y. Even our optimal fitting of the slope does not assure a consistent effective zero, as was also the case for the measurements of Reshotko and coworkers. Computations of the

displacement and momentum thickness and the shape factor $H = \delta^*/\theta$ carry some uncertainty. The scatter is expected to be larger for the profiles with larger extrapolation distance, i.e. for the recessed roughness configuration R1.

One can fit a series of such devloping profiles by several different families of analytical profiles surprisingly well with various optimization techniques. These fits would imply different virtual origins x_v of the profiles, different displacements from the true wall and slightly different pressure gradients; there is uncertainty in inference of the slope dU_0/dx from measurements of $V_0(x)$ in presence of some scatter, and some local blockage effects due to various supports. We suspect that many successful family fittings in the literature involve unacknowledged movements of inferred virtual origins which are hard to justify on rational grounds. Ultimately, we decided to compare the profiles purely qualitatively, in their dimensionless form as they are scaled with respect to δ^*, which is computed from each dimensional profile; see Fig. 1 for illustration of such profiles. This matter is dwelt upon because of the issue of the destabilization by roughness through changes in mean profile.

In Fig. 1 and all our other mean profiles there are no inflection points such as found by Kendall over his regular distribution of equal spherical elements. Reshotko and coworkers also found no inflection points, but that was before the Kendall experiments. Alerted to its possible occurrence, we were especially careful, but found no evidence of even a tendency toward inflection. We conjecture that the regularly arranged smooth spherical tops at precisely the same height lead to streamwise vortices at an essentially fixed y and these in term provide the regular extra eddy momentum transfer which inflects and bends the mean U(y) distribution. For Kendall's spheres we have $k_{nom} = k = k_{max}$. In our case the distribution of k among the randomly spaced roughness elements ($k_{max} \sim 1.5k_{nom}$) should provide a smoother average streamwise vorticity distribution in y so that the tendency towards inflection, if any, would be small. Furthermore, our nominal local k/δ^* values are more than twice those of Kendall, so that more of the flow is below the roughness peaks.

In terms of y/δ^* the TS critical layer in Blasius profiles for

the frequency with greatest amplification occurs at about 0.63 for Re_δ^* near 1000. For optimal indication of any possible TS waves the smoke wire had to be placed at about that height, rather close to the roughness peaks; then it could show the telltale vorticity-smoke concentrations in Kelvin's cat's eyes just above the critical layer, it and when they are present. Note that his happens in the linear range although nonlinearity must come in near the onset of secondary instabilities.

1.5 On measurement of amplification rates without a vibrating ribbon.

Consider now the issue of inferring amplification rates from measurements of disturbances over the smooth wall. It is interesting that no reliable data can be found in the literature, except when the excitation is controlled by a vibrating ribbon (or equivalent) which provides a truly dominant peak in the spectrum. With respect to this enhanced signal, u', as it is followed in an x-traverse from some initial value u_0', any increments which free-stream disturbances at that frequency might contribute are usually negligible. In the customary representation, such as Fig. 9, $\ln(u'/u')_0$ is plotted against x and the local slope yields the exponential amplification rate $-\alpha_i$, usually made dimensionless with δ^*. According to quasi-parallel theory $-\alpha_i$ varies with Re_δ^* from zero at the lower branch I of the neutral curve (See Fig. 8) to a maximum, roughly half way between the two branches, and decreases again toward zero at the upper branch II of the TS loop. Thus over small x distances, corresponding to the center of the TS loop, the plot is nearly a straight line with a slope of $-\alpha_{imax}$. Elsewhere the local slope of $\ln(u'/u_0')$ should be less.

It is important to emphasize that this interpretation is valid only when the perturbation u' grows directly from u_0' with no additional $\Delta u'$ excitation along the path. When we have excitation due to stochastic free-stream disturbances we must allow for the possibility that besides the TS self-amplification there is continuous influx of energy into the power spectrum of the disturbances in the boundary layer; the input is likely to be spread over most of the flow region and not localized as in the case of the vibrating ribbon. The spectra in Fig. 7 in fact represent averages over approximately 3

minutes, i.e. enough time for more than 7000 net TS wavelengths to pass by. Beyond this range of averages, no significant changes in the spectra were observed. Actually the patterns passing by comprise more or less randomly modulated wave packets in the TS excitable range and numerous less strucured patterns at other frequencies. This is partly confirmed by oscillographs, which were always monitored, but not shown here.

We observe from Fig. 7 and other spectra with roughness, that the spectral intensities rise with x even outside of the amplified TS range. One reason for the growth at lower frequencies is discussed in the next section. Another reason is the additional excitation between the x stations of the spectral sequence made easier by the low inertia region near the wall (expectation A of section 1.2). This additional excitation is not negligable relative to u'(f) as it is in the vibrating ribbon experiments over smooth walls. We should allow for the possibility that additional external excitation $\Delta u'(f)$ between x stations may be significant even in the region of TS amplification.

Where the total fluctuation level u'/U_0 remains below about 1%, the process we are observing is believed to be linear except for the possible occurrence of secondary instabilities (Herbert, Ref. 7). A telltale sign of such secondary instabilities is a sudden extra rapid rise in a lower frequency amplitude, f_2, while the amplitude of the highest frequency, f_1, which had been amplifying, starts leveling off or even decreasing. When $f_2 = f_1/2$ this is a powerful evidence for the onset of secondary parametric Craik instability, see Ref. 7. In such cases, $-\alpha_i$ is usually higher; but should not be compared to TS amplification, even though the corresponding F, Re_δ^* point may fall within the TS loop.

1.6 On non-TS growth at lower frequencies and three-dimensionalization

If the processes are linear, then the growth of the u' spectra outside of the TS range cannot be due to the turbulent-like three-dimensional vortex stretching. In Fig. 7 such low amplitude non-TS growth is quite substantial for the lowest part of the spectrum. A probable interpretation, consistent with our knowledge of hot-wire responce, is that this growth represents increasing three-dimensiona-

lization of the disturbances. In the terminology of turbulence, skew Fourier components may be growing and these would be sensed by a single hot wire as extra contributions at low frequencies because of aliasing. It would not be surprising if our roughness and non-uniformities in its spatial distribution would contribute to three-dimensionalization of the disturbances. The patterns of streamwise vortices (expectation A of Section 1.2) are "invisible" to the hot wire, when steady. Should they start weaving and meandering under the infuence of free-stream disturbances (expectation B), they would present highly skewed fronts to the hot wire and would register as low frequency u′ fluctuations. Hence the relative growth in the lower frequencies with roughness may be significant.

1.7 On occurrence of multiple TS peaks and of oblique skew waves.

We note that in the spectra at x=119 cm. in Fig. 7, there are five local peaks between 25 and 50 Hz, corresponding approximately to the TS excited range. In uncontrolled lower-disturbance environments two to three local peaks commonly occur in TS amplified range (our experience and unpublished results of Levchenko and Polyakov, and Arnal and Juillen). For a white free-stream disturbance spectrum theoretically the highest observed frequency peak would correspond to those essentially two-dimensional TS wave-fronts which are most amplified along a horizontal constant-frequency path in Fig.8 which ends at the upper branch II for any given Re_{δ}^{*}. The exponential amplification $A = \int_{I}^{II} \alpha(x)dx$ is maximal. As we have seen the integral does not take into account possible free-stream inputs along the path. And, of course, the external disturbance spectrum is not white. Careful studies of velocity and pressure spectra in our open-throat facility several years ago disclosed a spectrum which dropped monotonically from a maximum at f = 0 except for shallow local maxima near 11 and 22 Hz, the resonant frequencies in the room. Changes in the facility may have introduced some preferential frequencies; if so, they are not evident except after some selective amplification in the boundary-layer filter-amplifier.

There seems to be more such separate peaks in the spectra of the rough configurations (but the sample may be too small to generalize). In the Reynolds number range 900-1000, in Fig. 8, these peaks do not

superpose. They should coincide if they were driven by the same external spectrum; here we assume that the forcing spectra change only slowly with U_0 or with x, and therefore with Re_{δ}^*). Thus at least in the rough cases the peaks are more likely to correspond to surface conditions and hence are likely to be associated with locally oblique waves. One experimental check was made to investigate this possibility: the R1H spectrum of Fig. 7 at x = 126 cm were also taken at a spanwise station 3.5 cm off the centerline. The peak of the presumably two-dimensional TS wave at 50 Hz was at the 0.27 level, and its pure subharmonic at 26 Hz doubled; in contrast the presumably oblique wave at 38 Hz was nearly halved. Thus at z = 3.5 cm, there were apparently many more wave packets centered on 50 Hz and more frequent early secondary instablitiesof the Craik type, probably boosting the 26 Hz peak beyond the normal TS amplification rate. Unfortunately, there was not enough time to explore further these multiple peaks and their dependence on the free-stream and surface conditions.

1.8 On interpretation of visual and spectral evidence.

We may also ask whether the smoke-wire visualization should not clarify the issues of multiple peaks and skew wavefronts. Multiple frequency peaks imply multiple wave lengths. The height of the critical layer is a rather weak function of frequency and Re_{δ}^*, so that the smoke, emitted near the critical layer, should be able to participate in concentrations at the other wavelengths. But how should such a participation on the part of weaker motions look? A more disorderly, seemingly nonperiodic pattern? In any case, there is no consistent evidence for the presence of distinct superposed wave lengths. But the frequency peaks are certainly real!

Neither does there seem to be much visual evidence for substantial local obliquity of wave fronts at lower and moderate Reynolds numbers. One possible explanation would simply acknowledge the fact that the photographs represent a highly selected sample. They illustrate part-time occurrence of more organized structures rather than an average of all the configurations that float by during the time sample utilized in the spectral representation. A large enough

number of photographs are not kept and analyzed simply because "they don't show much". Keeping in mind that all the structures and events are superposed and randomly modulated, we cannot expect to observe for instance clear cut oblique waves correlated across the space of the test section. The unused sample of the unclear photographs may well correspond to more disorganized superposition of locally skew waves and waves with different wavelengths.

1.9 Key results and discussion

The issues associated with mean velocity profiles over distributed roughness were discussed in Section 1.4. Fig. 1 for the protruding roughness at the higher speed, R2H, is actually typical of the different developing families of profiles over distributed roughness (except that lower U/U_0 values were obtainable than for R1H and hence less scatter as commented in Section 1.4). Note that the triangles at $x = 48.4$ are for the smooth boundary layer just upstream of the roughness which commenced at $x_0 = 50$cm. The smoothed displacement thickness grows monstonically with x, and is consistently 1 - 2mm thicker than $\delta^*(x)$, for the smooth wall. The exception is at the last station where R1H is at least intermittently turbulent.

Section 1.4 discussed the care exercised in verifying that there was no tendency toward an inflection point; it also mentioned our conjectures, based on our experiences, concerning the genesis of the inflection in Kendall's profiles over the regular arrays of identical sphere elements. Fig. 1 superposes rather well on the family of higher-speed smooth-wall profiles (except that SWH has more scatter near the free stream).

A more quantitative measure of the tendency to instability of laminar profiles is the scale factor $H = \delta^*/\theta$, see discussion of Figs. 9a and 9b in Obremski, Morkovin and Landahl, Ref. 8. H for R2H exhibits some surveys, especially at $x = 83$cm and $x = 103$cm, but on the average is insignificantly higher (more unstable) than $H = 2.45$ for the smooth-wall profiles SWH. (Blasius profile has a still more unstable H of 2.6.)

Figs. 2 and 3 show the x-development of the total rms $u'(y/\delta^*)$ disturbance profiles for the higher-speed smooth-wall and recessed roughness configuration. (The 60 cycle-correlated contributions to u'

were eliminated by a special technique.) The growth for R2H is even higher than for R1H in Fig. 3. In Fig. 3 the development of the inner maximum near y/δ^* of 1 and the outer maximum above y/δ^* of 3 suggests strongly the build up of TS eigenfunctions for $|u|$. Keeping in mind the presence of broad band spectra in unstimulated u′ fluctuations, the weak growth of the inner peak in Fig. 2 indicates that there may be a slow development ot TS motions in the smooth-wall case as well. The TS nature of the growing fluctuations is characterized better by visualization techniques or through spectra.

In Fig. 4 the first light on the right is located at x = 127cm and the downstream one at x = 166cm; the flow is right to left. The smoke-wire traces in the upper figure record one of the more structured patterns of TS waves corresponding to the averages in Fig. 2. There is some three-dimensionality and some unevenness in wavelengths, as one would expect for an artificially unstimulated, freely growing TS wave packet pattern. The pattern discloses no suddenly growing three-dimensional formations, characteristic of secondary instability (as seen in the lower figure); the growth can well correspond to a linear regime.

The lower part of Fig. 4 corresponds to the u′ profile development of Fig. 3. Near x = 150cm triangular patterns at the bottom and at the center develop rather rapidly, indicating secondary instability and faster than TS growth. This is consistent with the shift of u'_{max} to $y/\delta^* = 2$ in Fig. 3. We may also suspect some turbulent breakdown near the second light at x = 166cm. We note that near this x value, $Re_{\delta}*$ for the R1H case is about 30% larger than that for SWH. For the R2H case the difference in $Re_{\delta}*$ is only about 10% so that the contrast in growth is more spectacular. The details of the triangle developments and possible first turbulent motions are discernible in Fig. 5, an enlarged view of a R1H condition.

The formations in Figs. 4 and 5 and in many other visualizations are similar to the patterns of Craik-type and Herbert-type instabilities as documented and discussed by Saric and Thomas, Ref. 9. Also the relatively low level of u'/U_0 at which these instabilities emerge is consistent with their findings. The Klebanoff-type in-line peak-valley configurations were never observed for unstimulated dis-

turbances. However, when the TS waves were driven at 30Hz at high amplitudes by a loudspeaker at x = 50cm in the wall opposite to the test wall, clear K-type breakdown was documented; see Fig. 15 in Bar Sever, Ref. 10. This again is in agreement with Saric and Thomas, Ref. 9. For discussion of the associated receptivity to sound, see part 2 of this Final Report.

Figs. 6 and 7 display on a linear scale the spectral development in x for the R1L and R1H cases, respectively. The solid lines represent $u'(f)/U_0$ at approximately y/δ^* of unity, the location of the inner u' maximum in the linear TS range. The dashed line in Fig. 6 indicates the free-stream spectra beyond the edge of the boundary layer. There, however, the outer TS eigenfunction lobe has not yet decayed to zero, so that when TS fluctuations strengthen, the spectrum no longer represents true free-stream conditions. Evidently, there are no preferred frequencies in the free stream except for the aforementioned 11Hz room-resonant frequency. The two-dimensional TS wave apparently grows at 30Hz, quite rapidly at first. The emergence of a second peak near 26Hz seems even more rapid and may possibly signal a subharmonic Herbert-type instability near x = 144cm. Actually the subharmonic 15-25 Hz band also grows steadily but does not form clear secondary instability peaks until x = 154cm. By x = 174cm, there must be substantial three-dimensionalization to lift the low frequencies so substantially but the slow growth beyond 30Hz suggests that the flow still has very few turbulent spots, if any. Later, in Fig. 10, we shall attempt to characterize the lower-speed amplifications, for R1L and R2L, in a more comprehensive manner.

The higher-speed spectra in Fig. 7 extend to higher frequencies as is consistent in the linear theory. For constant frequency and fixed x, the dimensionless coordinates in Fig. 8, F and Re_{δ}^* vary as $(U_L/U_H)^{3/2}$ and $(U_H/U_L)^{1/2}$. The upper branch II of the TS loop slopes less with increasing Re_{δ}^* than the constant f variation above. Then, in accordance with Section 1.7, the focus of maximum linear total amplification, F_{II}, R_{δ}^*, encompasses higher and higher dimensional frequencies. Simultaneously the dimensional amplified band width $F_I F_{II}$ broadens. The phenomenon of multiple peaks was discussed in Section 1.7. Thus already at x = 119cm in Fig. 7,

there is evidence of substantial selective amplification from 26Hz to 50Hz, the presumed two dimensional TS frequency corresponding to F_{II}. The 38Hz peak grows precipitously by x = 126cm, testifying to the presence of an early, highly amplifying secondary instability. The decay of the original 2D 50Hz wave by x = 136cm is coupled with a high rise of the subharmonic band near 26Hz, and of another low-frequency band near 12Hz. This should correspond to a more common occurrence of the halving Craik instability on one hand, and substantial three-dimensionalization on the other. Note the condensed scale at x = 154cm; there the broad band spectra appear turbulent with high intermittency, perhaps even fully turbulent. The different behavior at x = 126cm, 3.5cm off centerline, was described in Section 1.7, indicating substantial spanwise nonuniformity.

Fig. 8 pulls together the information concerning the various peaks that were followed in different regimes. The Blasius neutral loop made up of F_I and F_{II} merely frames the frequency and Reynolds number ranges. The shape factor information suggests that all mean profiles should be somewhat more stable than the Blasius profile, with the possible exception of recessed R_δ* profiles.

The contrast between the x-developments of the total u' for SWH and R1H in Figs. 2 and 3 testifies to the magnitude of the relative of the effect of the distributed roughness. For a more absolute measure we need to calibrate first the approximate smooth-wall amplification rates obtained in an unstimulated process where additional $\Delta u'(f)$ excitation between x stations may not be negligible with respect to $u'(f)$, as discussed in Section 1.5. Keeping in mind that the ridge of normal maximum amplification rate $-\alpha$ runs approximately half way between F_I and F_{II}, we should expect from the location of the SWH points in Fig. 8, that normally obtained amplification rates should be largely below this maximum. This normal maximum rate at Re_δ* of 1000 is indicated by the straight line with the dimensional slope of 0.3 per centimeter on the semi-logarithmic graph of (u'/u'_0) vs $x-x_0$. Here the reference location was chosen at x_0 = 119cm so that at $x-x_0 = 0$ all the u'/u'_0 developments start at the same normalized level of unity. We conclude that unstimulated growth with possible $\Delta u'$ along the path evidently exceeds somewhat the

expected normally obtained $-\alpha_i$ values. (Remember that H is approximately 2.45 and the profile somewhat more stable than Blasius.)

In the preceding, there is no claim that the artificially unstimulated growth yields reliable amplification rates from spectra. It is an approximate calibration which tells us that the growth with possible $\Delta u'(f)$ enhancement between stations for the smooth wall is somewhat higher than expected.

For the lower-velocity conditions with roughness, R1L and R2L, the choice of x = 136cm for x_0 brings the data together in a comprehensible manner. From the discussion of Figs. 6 and 7, we know that x = 136cm is close to or fully in the region where secondary instabilities are active. Therefore, the slope 0.55 per cm, indicated by the straight line in Fig. 10, should be more characteristic of secondary instabilities than of the primary TS instability corresponding to the slope of Fig. 9. Indeed this straight line organizes the data comprehensibly for $x > x_0$, except for the highest frequency $F = 1.24 \times 10^4$. However, amplitudes at that frequency are not expected to grow: this frequency now simply mediates the influx of the energy into the subharmonics. Again, the 0.55 slope in Fig. 10 is not intended to "measure" any amplification rates, merely to indicate that they are indeed much higher than in linear TS processes over smooth walls.

It is the rates upstream of x_0 = 136cm that should be compared with TS rates. A glance at the left side of Fig. 10, shows that they are all equal to or higher or even very much higher than the 0.55 slope on the right. To trace how this can happen, we must return to our description of the developments in Fig. 6 in this section and in its companion for R2L. Such high growths are indeed there, very much higher than for the smooth-wall immersed in the same disturbance environment! The unavoidable inference is that the extra growth is caused by the roughness in presence of free-stream disturbances. But how?

Before we return to that question, it should be reported that the growth for rough configurations at the higher speed, R1H and R2H, was even harder to encompass in a graph of the type of Fig. 9, than R1L and R2L of Figure 10. A study of our discussion of Fig. 7 illustra-

tes the reason: several different effects are present. Bar Sever in Ref. 10, offers an ordering with x_0 = 119cm. There are slopes near 0.55 per cm and near 0.88 per cm when secondary instabilities are present, and again much higher slopes starting at x_0 = 119cm to be compared in the TS growth. It is desirable to recall (Herbert, Ref. 7) that the theoretical amplification rates for secondary instabilities depend on more parameters than do TS rates, in particular on the amplitude of the primary wave when secondary growth commences. Bar Sever's multiple slope scheme is only a way of organizing the information.

For the responsible mechanisms we should look to the special features of boundary layers with distributed roughness, discussed in Section 1.2. There we were led to expect (A) some dynamics involving streamwise vorticity as influenced by the individual roughness elements and ever present non-uniformities in their x-z distributions, and (B) susceptibility of the lower-inertia fluid in the valleys between elements to free-stream disturbances which must be much higher than that on smooth walls without local separations. Property (B) almost surely contributes to a faster build up of disturbances internal to the boundary layer. It may also contribute to the $\Delta u'(f)$ increments between measuring stations, even as the earlier disturbances partake in the documented TS behavior. In the TS mechanism phase relationships are important so that much of the incremental $\Delta u'(f)$ may be wasted.

Given the "malleability" of low-inertia fluid near the wall and fact that the critical layer was just beyond the roughness peaks, could there be a condition for a more efficient TS mechanism? Perhaps vibrating ribbon experiments might elucidate that. (Artificial acoustic excitation did not help because it was not sufficiently pure and localized.)

Syndrome (A) almost surely intervenes in the latter stages of the growth as three-dimensionalization becomes more involved. Whether it could contribute earlier remains a question, difficult to test, theoretically or experimentally.

1.10 Conclusions and Recommendations

The effects of distributed roughness which starts at Reynolds numbers near or past R_{CrTS}, with initial k/δ^* o.. the order of 0.5, differs drastically from the TS bypass mode of Leventhal and Reshotko, Ref. 2, for smaller initial Re_{δ}^* and larger initial k/δ^* value and from the effects of isolated 3D roughnesses described in Section 1.1. Whether the roughness is recessed, R1, or protruding, R2, it operates through extra effective mechanisms involving TS waves and early Craik-type and Herbert-type secondary instabilities, Ref.7.

Even though the effective growth far exceeds the Blasius TS rates, the measured mean profiles show no tendency toward inflection. In fact, for the protruding roughness, R2, which causes faster growth than the recessed roughness, R1, the measured shape factor $H = \delta^*/\Theta$ is approximately 2.50 as compared to 2.45 for the smooth wall. This slight destabilization can never be responsible for the striking contrast of the growth of disturbances over R2 roughness and over smooth walls.

For explanations we must look to the special characteristics the boundary layers with distributed roughness (Section 1.2 and end of Section 1.9): (A) streamwise vorticity determined by the individual roughness elements on non-uniformities in their x-z distributions, and (B) susceptibility of the lower-inertia fluid in the valleys between elements to free-stream disturbances which is certainly much higher than the corresponding susceptibility of boundary layers over smooth walls without local separations. How these characteristics enter the enhanced growth processes remains uncertain.

1.11 References

1. Klebanoff, P. S. and Tidstrom, K. D.: Mechanism by Which a Two-Dimensional Roughness Element Induces Boundary Layer Transition. Physics of Fluids, Vol. 15, No. 7, pp. 1173-1188, 1972.

2. Leventhal, L. and Reshotko, E.: Priliminary Experimental Study of Disturbances in a Laminar Boundary Layer due to Distributed Surface Roughness. Case Western Reserve University Report FAS/TR-81-155, 1981. (Also Leventhal, L., M. S. Thesis, Case Western Reserve University, 1981)

3. Merkle, C. L., Tzou, K.,T-S., and Kubota, T.: An Analytical Study of the Effect of Surface Roughness on Boundary Layer Stability. Dynamics Technology, Inc., Report DT-7606-4, 1977.

4. Shin, H-W., Prahl, J. M. and Reshotko, E.: Experimental Study of the Effects of Surface Roughness on Laminar Boundary Layer Stability in Water. Case Western Reserve University Report FTAS/TR-82-157, 1982. (Also Shin, H-W., Ph. D. Thesis, Case Western Reserve University, 1982)

5. Kendall, J. M.: Laminar Boundary Layer Velocity Distortion by Surface Roughness: Effect upon Stability. AIAA Paper 81-0195, 19th Aerospace Sciences Meeting, Jan., 1981.

6. Thomas, A.S.W.: The Control of Boundary Layer Transition Using a Wave-Superposition Principle. J. Fluid Mech., Vol 137, pp. 233-150, 1983.

7. Herbert, Th.: Analysis of the Subharmonic Route to Transition in Boundary Layers, AIAA Paper 84-0009, 22nd Aerospace Sciences Meeting, Jan., 1984.

8. Obremski, H. J., Morkovin, M. V. and Landahl, M.: Portfolio of Stability Characteristics of Incompressible Boundary Layers. AGARDograph No. 134, NATO, Paris, March, 1969.

9. Saric, W. S. and Thomas, A. S. W.: Experiments on the Subharmonic Route to Turbulence in Boundary Layers. Proceedings IUTAM Symposium on Turbulence and Chaotic Phenomena in Fluids, Kyoto, Japan, September, 1983.

10. Bar-Sever, A.: Boundary Layer Transition Over Rough Surfaces. M. S. Thesis, Illinois Institute of Technology, May 1984.

1.12 Appendix I

Measuring the distance between the hot wire sensor and the rough surface, presented a special problem due to the fact that no clear y=0 point could be identified over the randomly distributed roughness pieces. A displacement indicator was used to determine a reference height above the rough wall for each measured profile. The indicator consisted of a one inch diameter (covering approximately 500 roughness particles) flat thin plate attached by a short spring to a 1/4 inch diameter rod, held parallel to the hot wire probe. When moved towards the sandpaper, the plate could pivot on the end of the spring so that it could adjust itself to the local highest roughness elements. A contact between the rod and the plate closed an electrical circuit and was easily detected by a continuity voltmeter.

The displacement indicator was calibrated over the smooth wall upstream of the roughness. This consisted of inserting the indicator until it contacted the measurement wall, indicated by electric continuity. At this point, a detent was machined in the indicator body which accepted the point of a set screw affixing the indicator securely to the traversing mechanism. With this point marked, the indicator was retracted so that a mean velocity profile could be taken. The distance between the indicator and the hot-wire sensor was determined by linearily extrapolating the velocity profile to determine the point at zero velocity. The distance between the extrapolated y-equal-zero point and the physical wall position from the indicator was recorded and used to obtain at every streamwise location, the true y position above the roughness peaks. After calibration the hot-wire probe was never loosened on the traversing mechanism. However, it was always necessary to retract the position indicator when acquiring profiles. The repeatability of locating the indicator calibration position with the set screw and detent was within an average error of 0.05 mm, or approximately 1/20th the height of an average roughness peak.

II. GENERATION OF INSTABILITY WAVES BY EXTERNAL UNSTEADY PRESSURE GRADIENTS

2.1 Some issues and some history

Sound falling upon a model in a wind tunnel is known to initiate the growth of instable Tollmien-Schlichting (TS) waves past the critical Reynolds number, Re_{cr}, at the frequency of excitation. This boundary-layer receptivity to sound has complicated the inference of the onset of transition to turbulence from many a wind-tunnel test. It is one of the serious obstacles to the NASA Laminar-Flow Aircraft Project because the sound intensity on the wing and fuselage in flight is considerable. It was the objective of the present project to clarify the controlling mechanism and the parameters of this receptivity.

Mathematically the problem was confusing because at the offending unstable TS frequencies, the acoustic wavelength λ_{ac} is always very much longer than λ_{TS}. Under such conditions, the transfer of energy or vorticity from the sound field to the TS field is believed to average out to practically nothing. Analysts like Goldstein (1983) and computation specialists like Murdock (1980) tried to simplify the problem by studying a sound wave at grazing incidence to a semi-infinite flat plate in the long-wave limit of the problem: $k = 2\pi/\lambda \to 0$ They concluded that coupling could occur only close to the leading edge where the boundary layer changed quite rapidly with x. However, excited TS waves there are damped and would decay by factors over 1000 before they could start amplifying past the critical Reynolds number at x_{cr}.

Many experimentalists, especially the Russians, looked to the leading edge itself for explanations. Kachanov, Kozlov and Levchenko (1975) even found convincing evidence that their flat plate vibrated under their relatively high acoustic forcing and that the vibrations of the leading edge of their one-centimeter thin plate caused the vorticity waves. Furthermore, sharp, completely rigid leading edges are mathematically singular; in inviscid flow an infinite response takes place at the edge under even mild asymmetric excitation. While viscosity, separation bubbles and finite radii of curvature reduce the

flow response to finite values, the problem remains experimentally and theoretically very difficult near the leading edge.

It is not functional to discuss the weaknesses of each of the experiments in the lengthy receptivity bibliography in the over fifteen Russian entries alone. However, no experimenter measured the forcing field around an exterior boundary of the boundary-layer region where the TS response starts and grows; in other words the true forcing boundary conditions were always left undefined. A hot-wire on a x-y traversing mechanism can furnish such information because at low subsonic speeds a hot wire senses acoustic velocities very well. The real experimental difficulty is encountered inside the boundary layer, where the exciting signal, the response signal, and any parasytic signals are all superposed and cannot be rationally separated.

2.2 Key ideas for the design of the receptivity experiment

Past experiments and theory which experienced receptivity had one feature in common: an x-dependence of the driving field or the receiving field or both. This was our clue. We tried to construct an experiment which would have the amplitude A(x) of the pressure gradient x-dependent while avoiding the singularities of the leading edge. We settled on a local source of sound in the free stream, "radiating" onto the developed boundary layer on the sidewall of the IIT Visualization Facility.

The source provided the x-dependence of sound intensity along the well-investigated Blasius boundary layer on the wall. Because the receiving layer was in the near field, the required speaker power was so low that we could not hear whether it was on or off. The low power always kept us in the linear range and precluded the vibration problems that plagued other experiments. There was, of course, no problem with the leading edge of the plate and we could document and define the forcing field on the outside of the receiving boundary layer. Because of the superposition of the forcing and responding field it took us some time to understand the developments and form several firm concepts. Let us introduce them now.

2.3 Concepts developed during the experiments

An acoustic field is irrotational except at a wall where it acquires an acoustic vorticity sublayer because of the no-slip conditions. This sublayer is identical to the unsteady Stokes vorticity layer in the long-wave limit and trails the sound wave as the wave moves along a surface. On the other hand, TS waves are quint essentially vortical. It is then logical to look to the wall for the coupling of the driving sound to the responding vorticity field.

Mathematically, we have a forced, i.e., nonhomogeneous problem for the perturbations of a Navier-Stokes system within a rectangle of height, say 2δ, and length from x_0 far upstream of the source to $x_0 + L$ somewhere downstream of the source. Within the rectangle the system of differential equations is homogeneous as are the boundary conditions at the wall. Nonhomogeneity or forcing comes from the prescription of the oscillatory pressure field along the remaining three sides of the rectangle. The solution will consist of a "particular" or "nonhomogeneous" solution of the differential equations (which we shall call the forcing pressure, velocity and vorticity fields p_f, u_f, v_f, ζ_f) and a collection of response solutions of the homogeneous system, i.e., eigenfunctions. Above Re_{cr} the homogeneous solution that can grow is the TS solution with fields p_{TS}, u_{TS}, v_{TS}, and ζ_{TS}. The rest of the collection of the homogeneous solutions, designated by p_d, u_d, v_d, ζ_d, is always decaying and is in principle constructable from the contributions of all the higher damped TS modes and of the continuous spectrum functions discussed by Grosch and Salwen (1980).

For specific flow conditions: a given circular frequency ω and a local displacement thickness δ^*, the eigenfunctions of the TS and d fields should be fixed by the dimensionless frequency $F = \omega\nu/U^2$ and the Reynolds number $U\delta^*/\nu$. In principle then, for a given F and Re_{δ^*} only the amplitude and phases of these homogeneous solutions are unknown a priori. As in other nonhomogeneous problems, these should be determinable from the requirement that the total solution satisfies all the appropriate boundary conditions. As already discussed the wall boundary condition in particular could be expected to provide the link which would determine the amplitudes and phases of the TS and d fields in terms of the driving f field characteristics.

2.4 The wall boundary condition and the effect of variable pressure gradient

The simplicity of the no-slip wall boundary condition is deceiving. In fact when we set u and v to zero in the x-momentum equation we arrive at a fundamental constraint which must always be satisfied, for steady or unsteady flows:

$$-\nu \frac{\partial \zeta}{\partial y} = +\nu \frac{\partial^2 u}{\partial y^2} = \frac{1}{\rho} \frac{\partial p}{\partial x} \quad \text{at} \quad y = 0 \tag{2.1}$$

Since according to Fuchs law the term on the left represents the flux of vorticity diffusing out of the wall, any pressure gradient impinging on a rigid surface generates wall vorticity sources per unit area, per unit time equal to its amplitude, divided by the density ρ. In fact it is this link which ties the acoustic Stokes sublayer to any sound wave at the wall.

Equation (2.1) could serve as a boundary condition for the vorticity equation. If we average (2.1) over one period of the forcing frequency, these linear periodic functions yield zero. To see whether we can cummulate some effects on the average, we multiply (2.1) by ζ and again average over one period to obtain

$$-\nu \frac{\partial \overline{\zeta^2}}{\partial y} = \frac{2}{\rho} \overline{\frac{\partial p}{\partial x} \zeta} \tag{2.2}$$

for the source of mean square vorticity $\overline{\zeta^2}$ diffusing out of the wall per cycle, per unit area. The basic problem of non zero input from the forcing field to the TS field can be illustrated through the nature of the cross-correlation $C = \overline{(\partial p/\partial x)_f \cdot \zeta_{TS}}$ in (2.2) for the long-wave limit. In this limit the complex representation of the pressure gradient with constant amplitude A is A exp $(-i\omega t)$, and the corresponding expression for ζ_{TS} is ζ_{TS0} exp $i(k_{TS}x - \omega t)$ The average correlation C is then A Re$(\zeta_{TS0} \exp ik_{TS}x)$ which represents a purely periodic variation in x. When this quantity is averaged over one TS wavelength it yields zero, i.e., forcing pressure gradients with constant amplitude cannot generate $\overline{\zeta_{TS}^2}$ at the wall.

When the amplitude of the pressure gradient is x-dependent, A(x), the average cross correlation C will cease to be purely oscillatory as above. To see that let the Fourier transform of A(x) be $A_F(k)$, so that $2\pi A(x) = \int_{-\infty}^{+\infty} A_F(k) \exp ikx\, dk$. If $A_F(k)$ has a non-zero contribution at the TS wavenumber, i.e., if $A_F(k_{TS}) \neq 0$, there arises a net input rate from the forcing field to the TS field per cycle, per unit area, $C = Re[A_F(k_{TS})\zeta^*_{TS0}]\ \Delta k/2$, where z* is the complex conjugate of ζ and Δk is an effective bandwidth. This is the mathematical crux of the feasability of receptivity to sound.

In other words, the mismatch of the characteristic length λ_f of the sound field and λ_{TS} leads to cancellation of the input average, when the amplitude A of the forcing sound is constant. With a variable A(x), however, λ_f ceases to be the sole acoustic characteristic length. The Fourier spectrum of A(x) in effect measures the "spread" over other scales. If it overlaps with the k_{TS} scale, there is a positive input on the average.

The input at the wall is not the only mechanisum for increasing ζ . In the equation for ζ itself there is a term vU'' which represents the rate of transfer from the steady mean flow vorticity to the unsteady vorticity. When the equation for $\overline{\zeta^2}$ is formed by multiplying by ζ and averaging over the forcing period this term becomes $v\zeta\, U''$. The conditions for the transfer to $\overline{\zeta^2_{TS}}$ from the mean flow by the v_f forcing motion comes to the condition for non zero cross-correlation $\overline{v_f \zeta_{TS}}$. The amplitude A_f of v_f is proportional to $A'(x) + ikA(x)$ However, since the Fourier transform of $A'(x)$ is $ikA_F(k)$, the cross-correlation again is non zero when $A_F(k_{TS}) \neq 0$.

One can also write down a formula for the total contribution from the v_f motion, integrated over the boundary layer; but that adds little new insight. What is meaningful is that because of this input there can be a build-up of $\overline{\zeta^2_{TS}}$ far from the wall, long before any diffusive effect could reach there.

2.5 Evidence for the proposed concepts

Any general analytical solution for the f, TS, and d fields is not on the horizon. At present we can try to verify different features of these fields in specific solutions; i.e., in physical and numerical experiments. At our instigation Professor H. Fasel of the

University of Arizona carried out a difference solution of the Navier-Stokes equations for which the nonhomogeneous forcing boundary condition was purposely shifted to the wall. Specifically a local oscillating vorticity source $-\nu\partial\zeta/\partial y$ at the wall was prescribed to be zero except for a narrow strip where it was proportional to $\sin m\,(x-x_1)\cos \omega t$. The strip was made narrow so that the Fourier transform of $\sin m\,(x-x_1)$, would be broad and cover k . This indeed happened and a vigorous TS wave with a wavelength just over twice the strip width grew within two TS wavelengths. The $\overline{v\zeta}\ U''$ build-up of the vorticity farther away from the wall clearly contributed to the rapid growth. It was possible to identify the f and TS field by their evolutionary behavior. The d field could not be identified as such, but it must be present.

While in the numerical experiments the total u, v, and ζ fields were available from the computer, in our laboratory experiments only the information on the total u field could be obtained. We could identify $u_f + u_d$ fields far upstream (they were essentially Stokes-like near the wall). We did trace the expected change from Stokes-like profiles to those with increasing u_{max} at higher y locations as the TS field grew. Farther downstream, as the ratio $|u_{TS}|/|u_f|$ became large the phase speed approached that of TS waves. When we halved the free-stream speed without changing the forcing field, the response collapsed to an essentially Stokes-like behavior throughout. In the terminology of the preceding Section, $A(x)$ and $A_F(k)$ remained the same, but $A_F(k)$ could not overlap with any k_{TS} wavenumbers because at this lower speed the boundary layer was subcritical and stable. Thus the TS field became part of the d field and only $u_f + u_d$ was identifiable.

The details of both the physical and numerical experiments will be found in the paper by Nishioka and Morkovin under revision, aimed at the Journal of Fluids Mechanics. Here we can only outline the issues, the useful new concepts, and their verification in qualitative terms. However, it should be stressed that the often puzzling results reported in the earlier literature appear consistent with the views presented here whenever the forcing remained linear.

2.6 References

1. Goldstein, M.E.: The Evolution of Tollmien-Schlichting Waves Near a Leading Edge, J. Fluid Mech. Vol. 127, pp. 59-81, 1983.

2. Grosch, C.E. & Salwen, H.: Eigenfunction Expansions and Boundary-Layer Receptivity in the Theory of Hydrodynamic Stability, Int. Congress Appe. Mech., 1980.

3. Kachanov, Iu.S., Kozlov, V.V., and Levchenko, V.Ia.: Generation and Development of Small Disturbances in Laminar Boundary Layers under the Action of Acoustic Fields, in Russian, Izv. Sibir. Otdel. USSR. Acad. Sciences, Novosibivsk No. 13-3, pp. 18-26, 1975.

4. Murdock, J.W. (1980): The Generation of Tollmien-Schlichting Wave by a Sound Wave, Proc. Ray Soc. London A. Vol. 372, p. 1517, 1980.

TABLE I

Comparison of Flow Parameters

Exp.	Rough. No.	$Re_{\delta_0^*}$	Re_{k0}	k/δ_0^*	$(Re_{\delta^*})_{TS}$	$(Re_{\delta^*})_{TURB}$
Current	1	859	131	0.51	1025-1170[+]	1240-1380[+]
Current	2	875	143	0.50	961-1030[+]	1060-1100[+]
Current	1	725	101	0.48	915-990[+]	-
Current	2	704	101	0.44	760-820[+]	-
L & R	-	285[*]	314	1.48	-	Below 490[**]
L & R	-	480[*]	192	0.88	-	Below 600[**]

\+ Observed ranges.
* Assuming U = 6m/s, $\nu = 1.48 \times 10^{-5}$m/s.
** Based on undisturbed laminar flow.

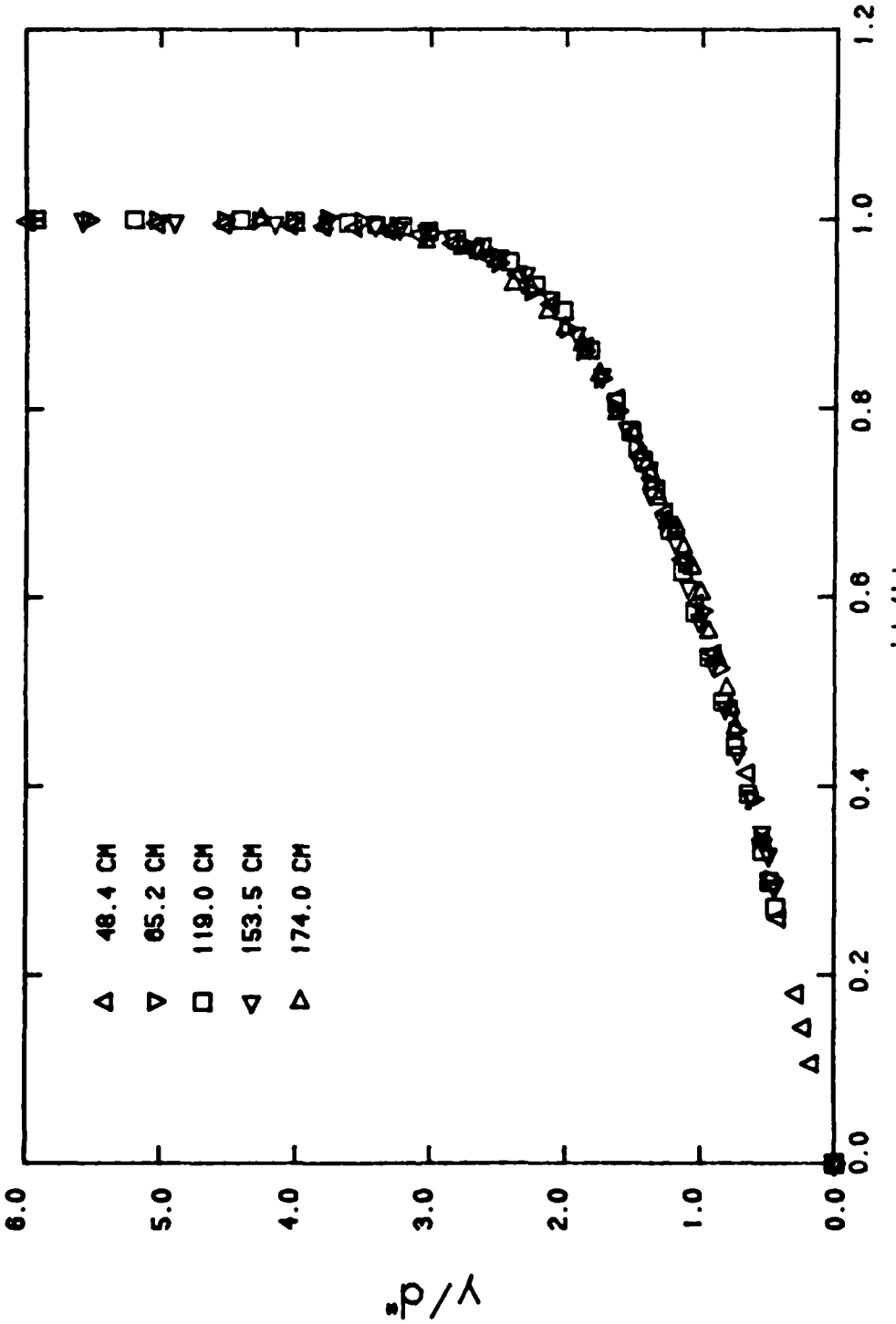

Figure 1. Mean Velocity Profiles Measured Along Rough Wall # 2 for the High Reynolds Number Condition

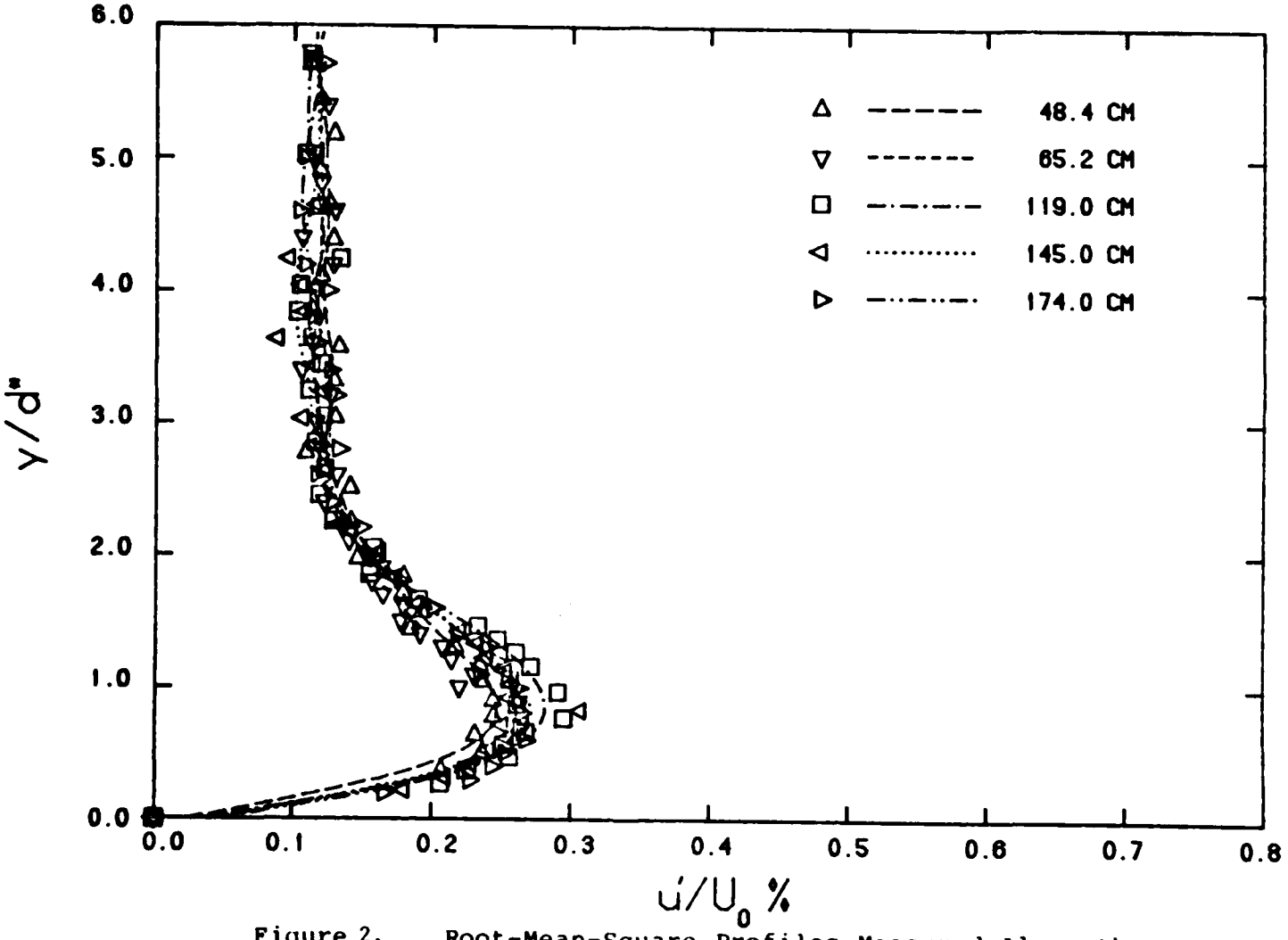

Figure 2. Root-Mean-Square Profiles Measured Along the Smooth Wall for the High Reynolds Number Condition

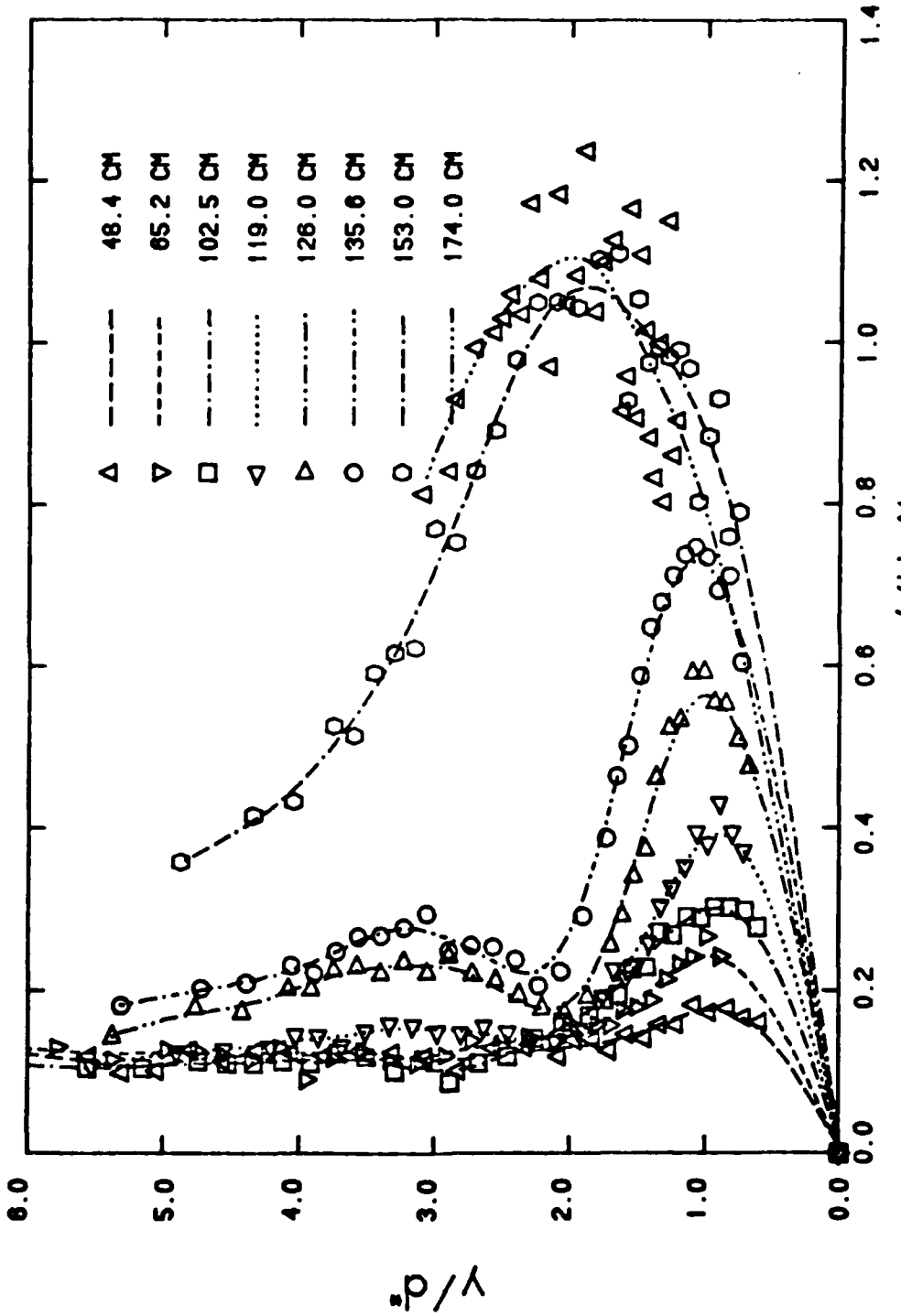

Figure 3. Root-Mean-Square Profiles Measured Along Rough Wall # 1 for the High Reynolds Number Condition

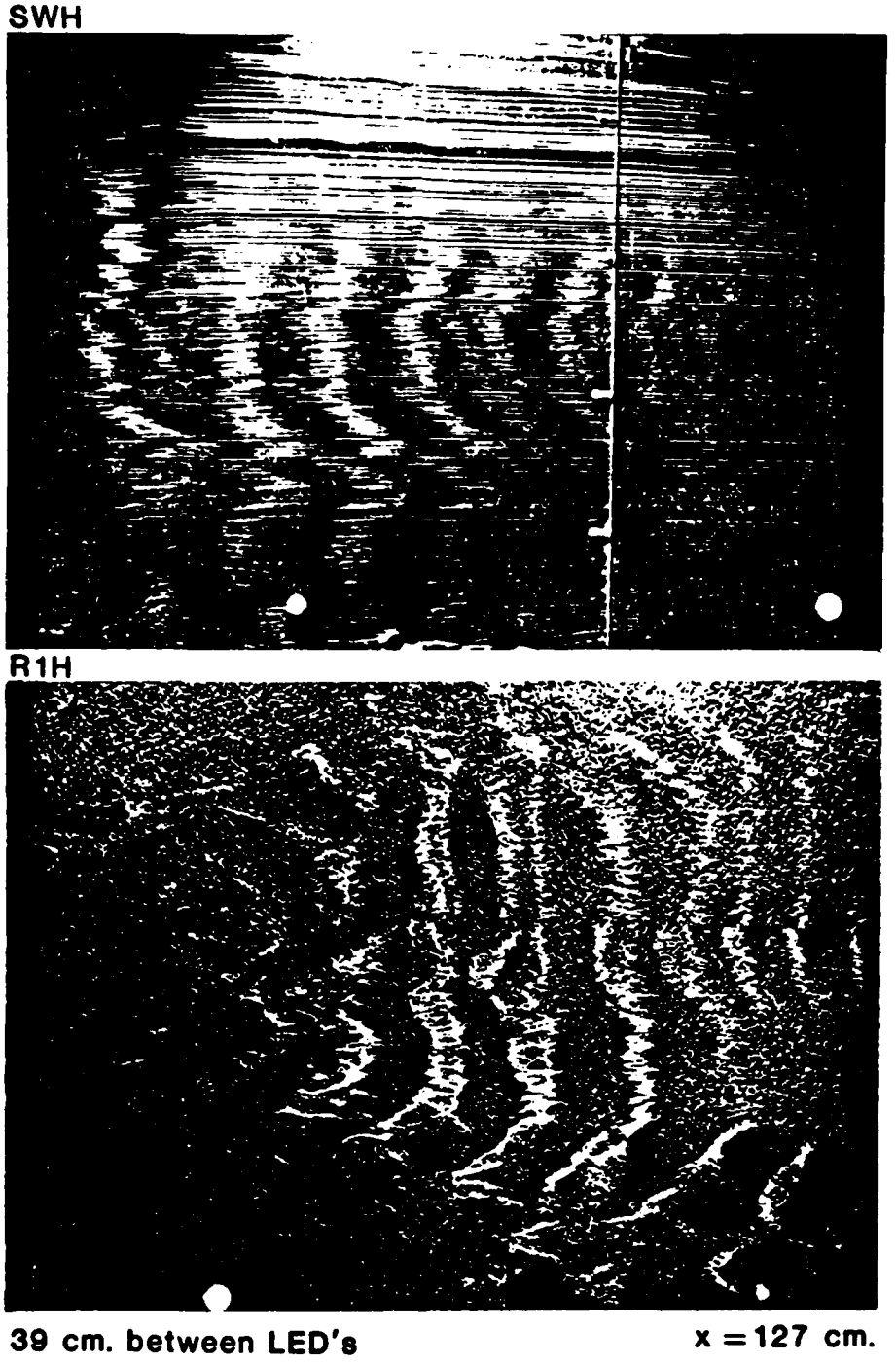

Figure 4. Visual Record of the Boundary Layer Flow Over the Smooth Wall (top), and Over Rough Wall # 1 (bottom) for High Reynolds Number Condition

R1H

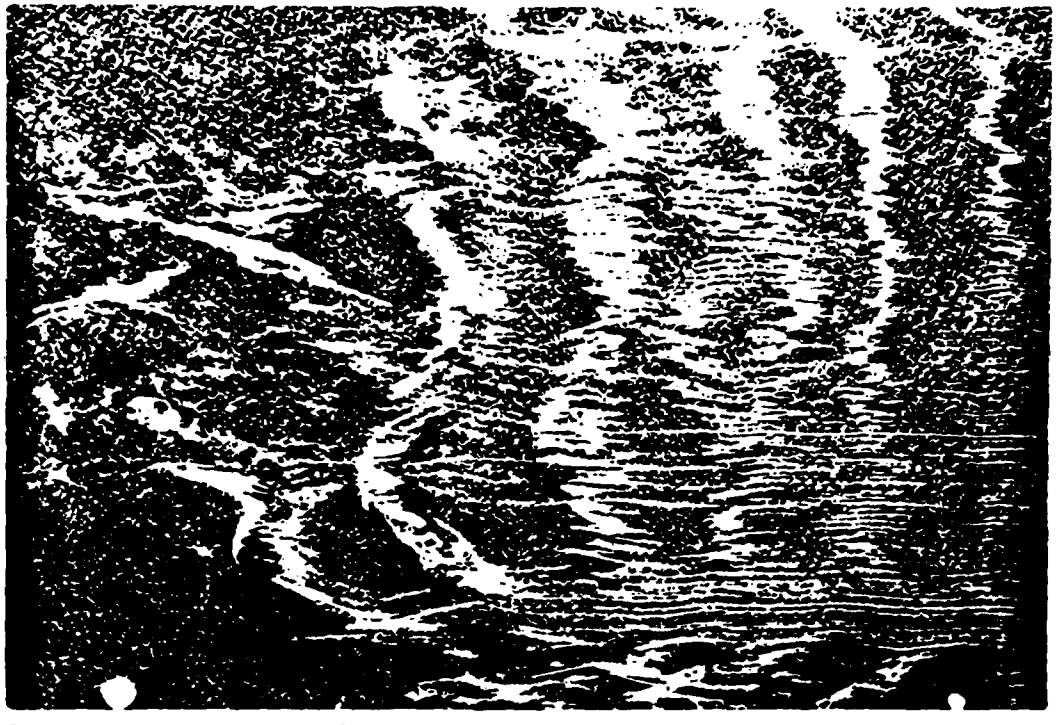

39 cm. between LED's x = 127 cm.

Figure 5. Enlarged Visual Record of the Boundary Layer Flow Over Rough Wall # 1 for High Reynolds Number Condition

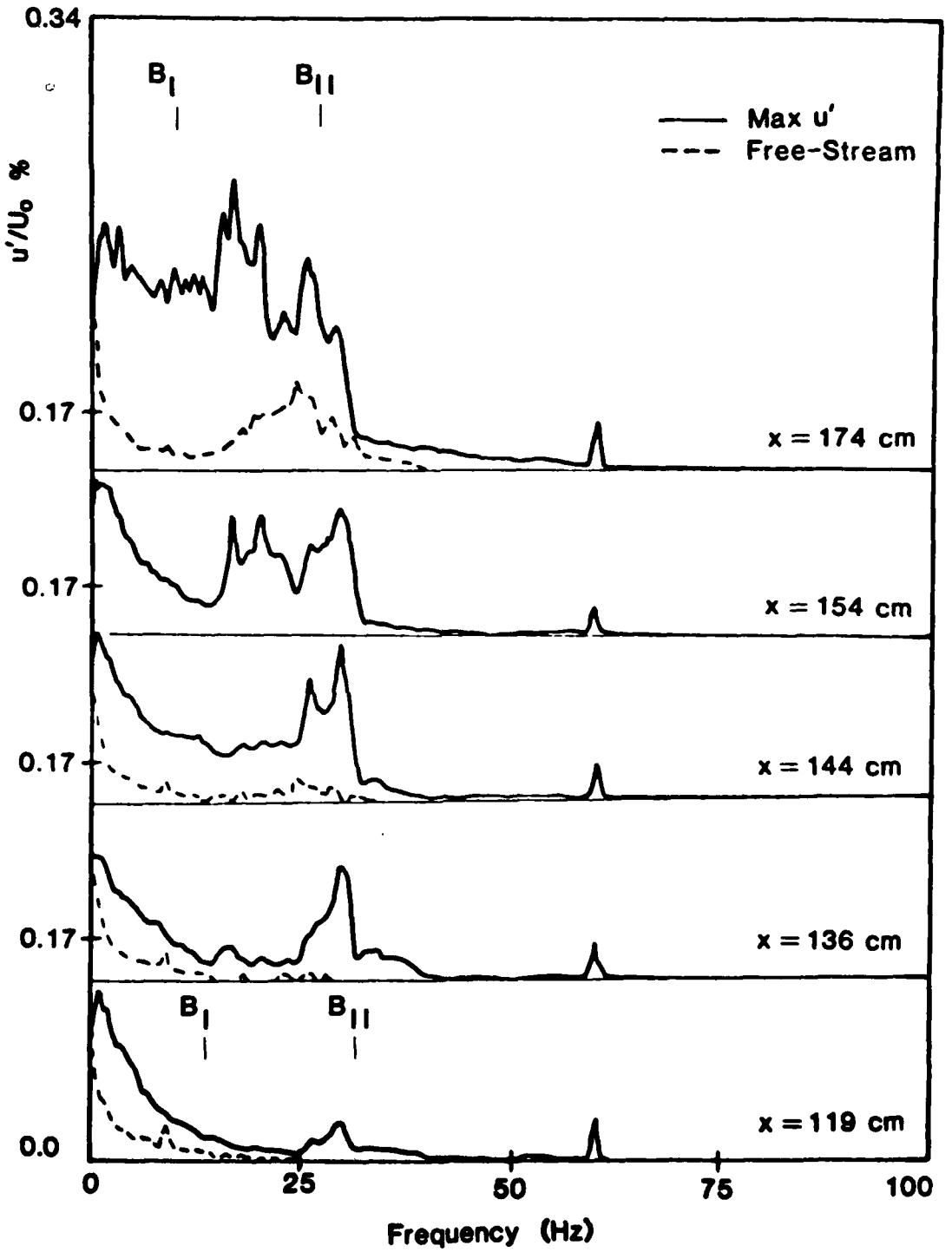

Figure 6. Spectra Development Measured Along Rough Wall # 1 for the Low Reynolds Number Condition

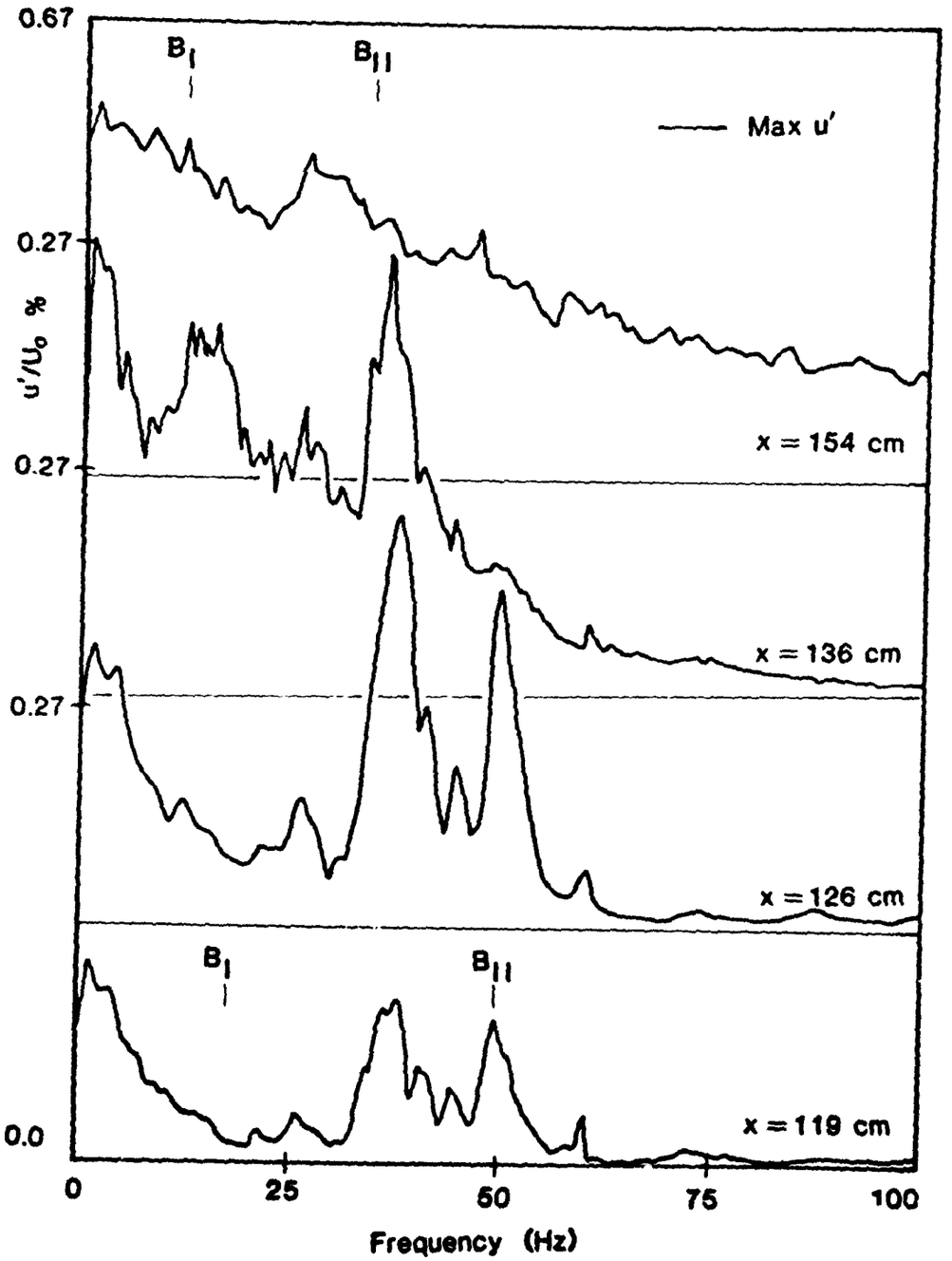

Figure 7. Spectra Development Measured Along Rough Wall # 1 for the High Reynolds Number Condition

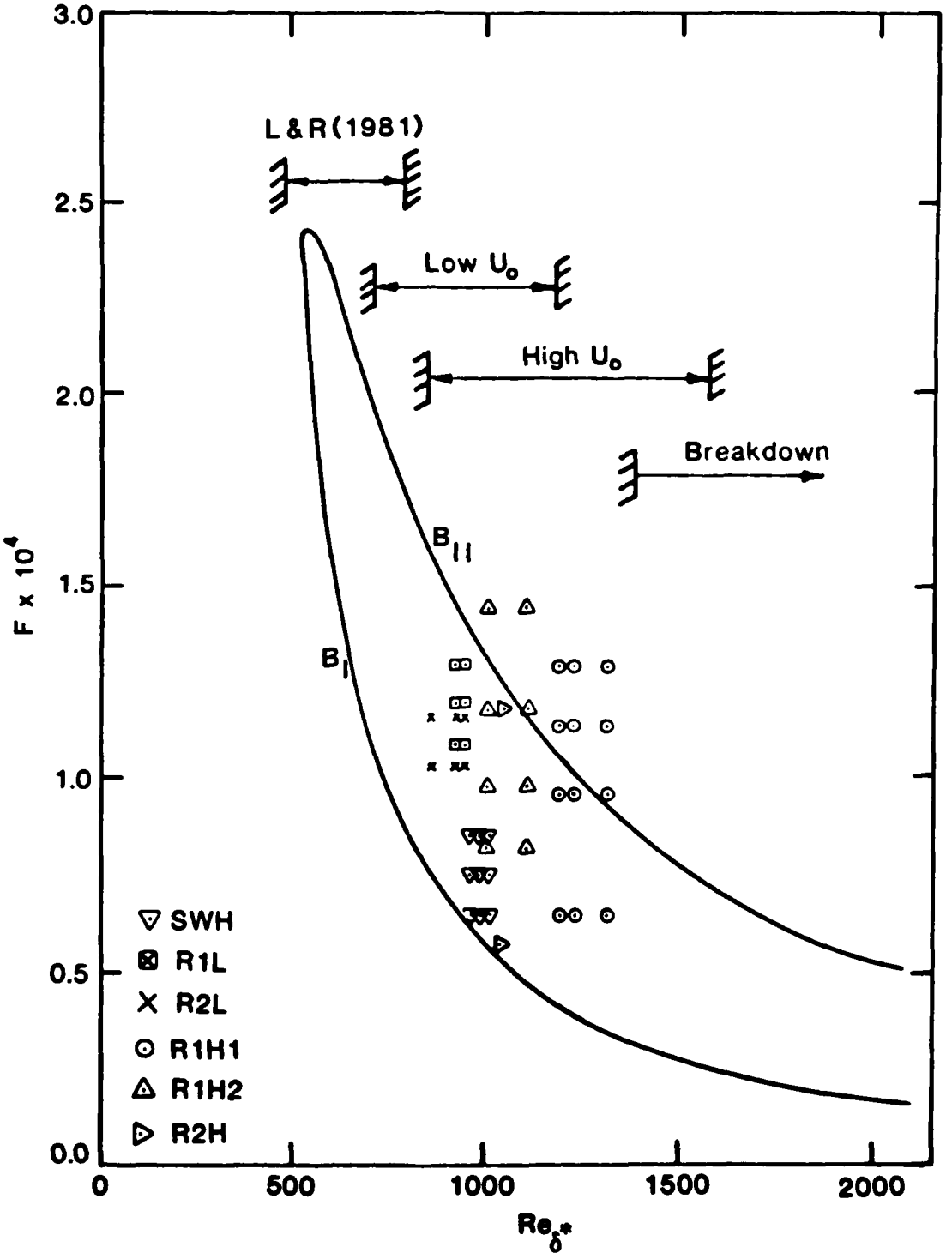

Figure 8. Distribution of Experimental Data on a Blasius Neutral Stability Curve

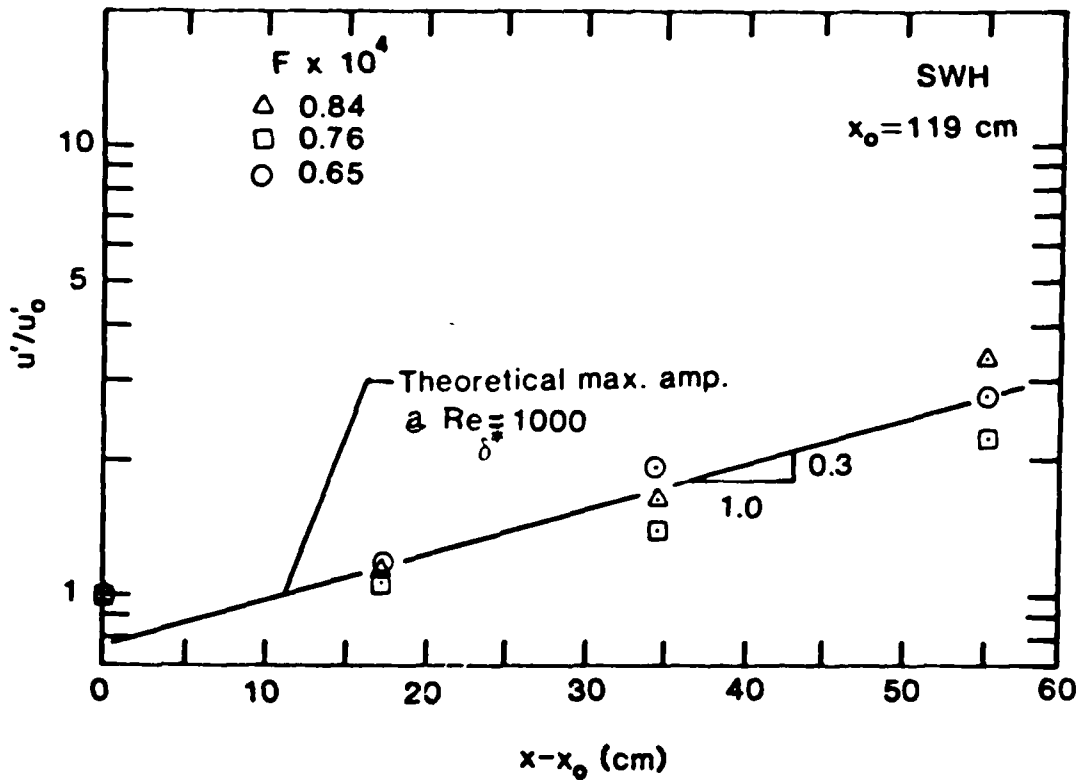

Figure 9. Disturbance Growth Characteristics of Boundary Layer Flow on the Smooth Wall for the High Reynolds Number Condition

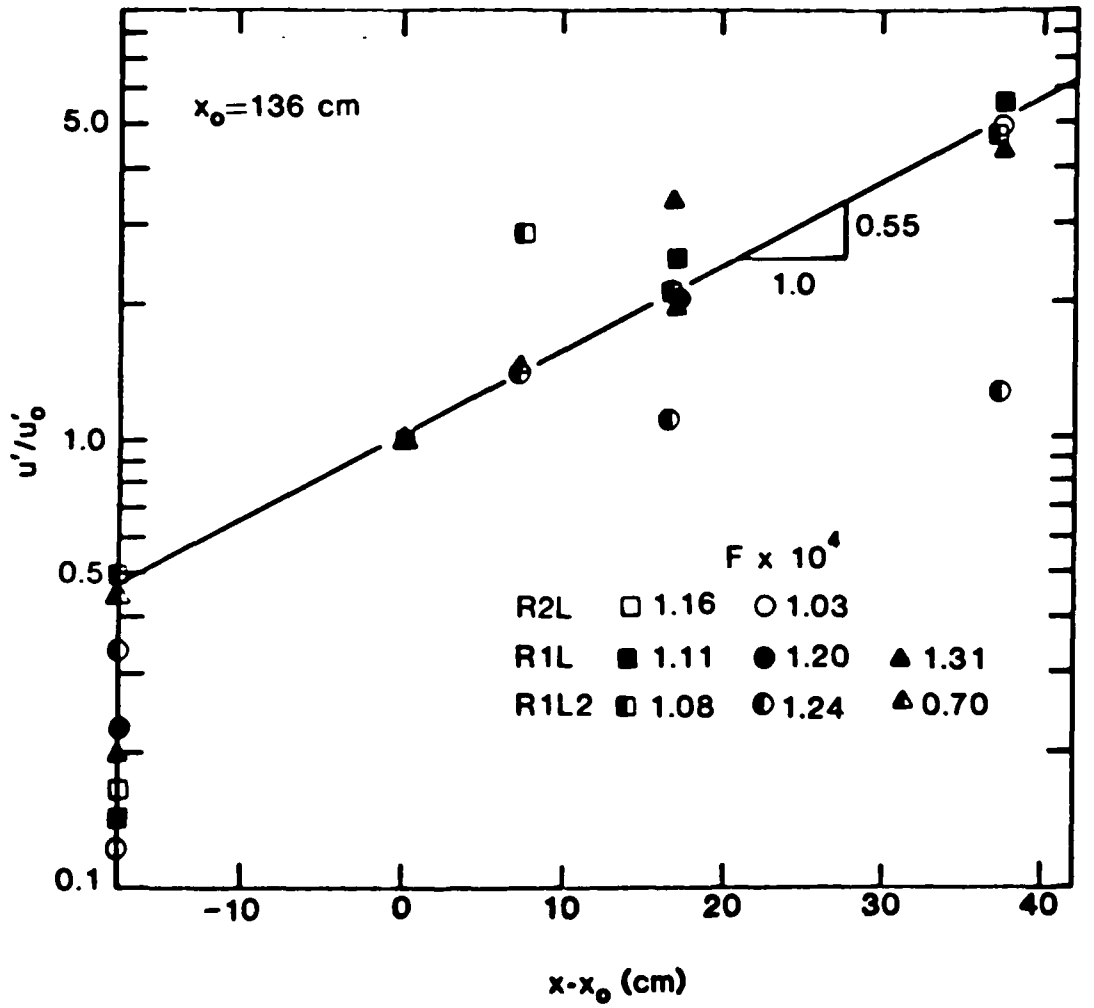

Figure 10. Disturbance Growth Characteristics of Boundary Layer Flow on the Rough Walls for the Low Reynolds Number Condition